Original Article

HIV-infected patients with opportunistic pulmonary infections misdiagnosed as lung cancers: the clinicoradiologic features and initial application of CT radiomics

Weiya Shi[1#], Lingxiao Zhou[2#], Xueqing Peng[2], He Ren[2], Qinglei Wang[3], Fei Shan[1], Zhiyong Zhang[1,3,4], Lei Liu[2], Yuxin Shi[1]

[1]Department of Radiology, Shanghai Public Health Clinical Center, Fudan University, Shanghai 201508, China; [2]Institutes of Biomedical Sciences, Fudan University, Shanghai 200032, China; [3]Department of Radiology, Zhongshan Hospital, Fudan University, Shanghai 200032, China; [4]Headmaster's Office, Fudan University, Shanghai 200433, China

Contributions: (I) Conception and design: W Shi, F Shan; (II) Administrative support: F Shan, Z Zhang, L Liu, Y Shi; (III) Provision of study materials or patients: W Shi; (IV) Collection and assembly of data: W Shi, L Zhou, H Ren, Q Wang; (V) Data analysis and interpretation: W Shi, X Peng; (VI) Manuscript writing: All authors; (VII) Final approval of manuscript: All authors.

[#]These authors contributed equally to this work.

Correspondence to: Fei Shan; Zhiyong Zhang. Department of Radiology, Shanghai Public Health Clinical Center, Fudan University, No. 2901, Caolang Road, Jinshan, Shanghai 201508, China. Email: shanfei@shphc.org.cn; zhangzy@fudan.edu.cn.

Background: To characterize clinicoradiologic and radiomic features for identifying opportunistic pulmonary infections (OPIs) misdiagnosed as lung cancers in patients with human immunodeficiency virus (HIV).

Methods: Twenty-four HIV-infected patients who were misdiagnosed with lung cancers on CT images and had OPIs confirmed by pathological examination or integration of clinical and laboratory findings and 49 HIV-infected patients with lung cancers confirmed pathologically were included. Semiautomated segmentation of the lesion was implemented with an in-house software. The lesion boundary was adjusted manually by radiologists. A total of 99 nonenhanced-CT-based radiomic features were then extracted with PyRadiomics. The clinicoradiologic and radiomic features were compared between the OPI and cancer groups.

Results: In the OPI group, 19 patients (79.2%) had tuberculosis (TB) infections, 2 (8.3%) had nontuberculosis mycobacterium (NTM) infections, 2 (8.3%) had cryptococcus infections and 1 (4.2%) had a mixed infection of TB and NTM. There were significant differences in age, proportion of smokers, smoking index, highly active antiretroviral therapy (HAART) duration, $CD4^+$ counts and $CD4^+/CD8^+$ ratio between the two groups (P=0.000, 0.012, 0.007, 0.002, 0.000, and 0.000, respectively). In peripheral-type lesions, the presence of pleural indentation was less common, and the presence of satellite lesions was more common in the OPI group (P=0.016 and 0.020, respectively). Four radiomic parameters of central-type lesions were significantly different, including large dependence high gray level emphasis (LDHGLE), skewness, inverse difference normalized (IDN) and kurtosis (P=0.008, 0.017, 0.017, and 0.017, respectively). However, neither CT features of central-type lesions nor radiomic parameters of peripheral-type lesions were significantly different between the two groups.

Conclusions: Clinicoradiologic features together with radiomics may help identify OPIs mimicking lung cancers in HIV-infected patients.

Keywords: Human immunodeficiency virus (HIV); X-ray computed tomography; opportunistic pulmonary infection (OPI); lung cancer; radiomics

Submitted Apr 27, 2019. Accepted for publication Jun 03, 2019.
doi: 10.21037/jtd.2019.06.22
View this article at: http://dx.doi.org/10.21037/jtd.2019.06.22

Introduction

The human immunodeficiency virus (HIV) and acquired immunodeficiency syndrome (AIDS) pandemic has entered its 4th decade. Due to the effectiveness of highly active antiretroviral therapy (HAART), the incidence of new HIV infections has declined, and the number of AIDS-related deaths in adults and children worldwide has plateaued (1).

However, the respiratory system is still one of the most frequently affected organ systems in HIV-infected patients, and opportunistic pulmonary infections (OPIs) remain a major threat (2). The pathogens may be bacteria, mycobacteria, fungi, or viruses. Several pulmonary infectious diseases occasionally cause inflammatory lung lesions resembling malignancy on images (3-7). Despite improvements in imaging techniques and serologic/microbiologic testing, accurate diagnosis remains challenging, and the diversity of infectious agents adds further difficulty (3). Since the management and outcome of OPI and cancer are entirely different, improving diagnostic accuracy is critical (3).

By visually assessing the CT images, we may miss information that is important in defining lesions. Radiomics, which is defined as the high-throughput automated (or semiautomated) extraction of large amounts of quantifiable information from a region of interest (ROI) on radiographic images, has attracted much attention (8). Radiomics is designed to decode the intrinsic heterogeneity of a lesion to improve management (9-11). Recent studies have revealed that radiomic analysis shows promising potential for differentiating lung cancers from benign pulmonary nodules (12-15).

To date, however, few studies have compared the clinical and radiological findings of masses or nodules caused by OPIs with the findings in lung cancers, and no research has been carried out, especially in HIV-infected patients. Therefore, we hypothesized that clinicoradiologic features together with radiomics might help identify these unusual OPIs in HIV-coinfected patients. In this retrospective study, we characterized clinicoradiologic features for differentiation and evaluated the feasibility and practicality of initial application of CT radiomics in these cases.

Methods

Patient selection and medical records

A search of the database maintained by the Department of Radiology in our hospital was conducted to identify HIV-infected patients who were initially misdiagnosed with lung cancers on CT images and had OPIs eventually confirmed by pathological examination or integration of clinical and laboratory findings during June 2013 and February 2018. HIV-infected patients with lung cancers confirmed by pathological examination were included as a control group. Twenty-four patients with OPIs and 49 patients with lung cancers (50 main lesions) were identified according to a patient selection flow chart (*Figure 1*) and included in the current study. The medical records of these patients were then reviewed, with particular attention to age at diagnosis, gender, smoking history, HAART duration, $CD4^+$ counts, $CD4^+/CD8^+$ ratio, histological types or laboratory findings, and follow-up or treatment outcomes. Staging was based on either the International Association for the Study of Lung Cancer tumor node metastasis classification for non-small cell lung cancer (NSCLC) or the Veterans Administration Lung Study Group criteria for limited disease and extensive disease for small cell lung cancer (SCLC) (16,17). The Institutional Review Board of Shanghai Public Health Clinical Center, Fudan University approved the study protocol. Informed consent was waived because of the retrospective nature of the study.

CT scans and image interpretation

The patients were examined in the supine position with their arms extended overhead. Scans were obtained from the thoracic inlet to the inferior portion of adrenal gland with a suspension after the end of inspiration. CT scans were performed with 1 of 2 scanners (Siemens Sensation 16, Siemens Medical Systems, Forchheim, Germany; or Hitachi Scenaria 64, Hitachi Medical Systems, Tokyo, Japan) using automatic exposure control with the following parameters: tube voltage, 120 or 140 kV; tube current, 160 to 250 mA; detector collimation, 16×0.75 mm, 64×0.625 mm; beam pitch, 1 or 1.0781; rotation time, 0.5 seconds; field of view (FOV), 350 mm; and matrix, 512×512. Images were reconstructed using a lung standard algorithm with 1-mm slice thickness at 1-mm intervals and displayed with lung window (–600/1,200 HU) and mediastinal window (40 HU/350 HU) settings.

The CT images were analyzed independently by two radiologists (W Shi and F Shan, with 10 and 17 years of experience in chest radiology, respectively), who evaluated images without any previous knowledge of the patients' clinical or laboratory findings. In cases of disagreement, results were obtained by consensus between the two

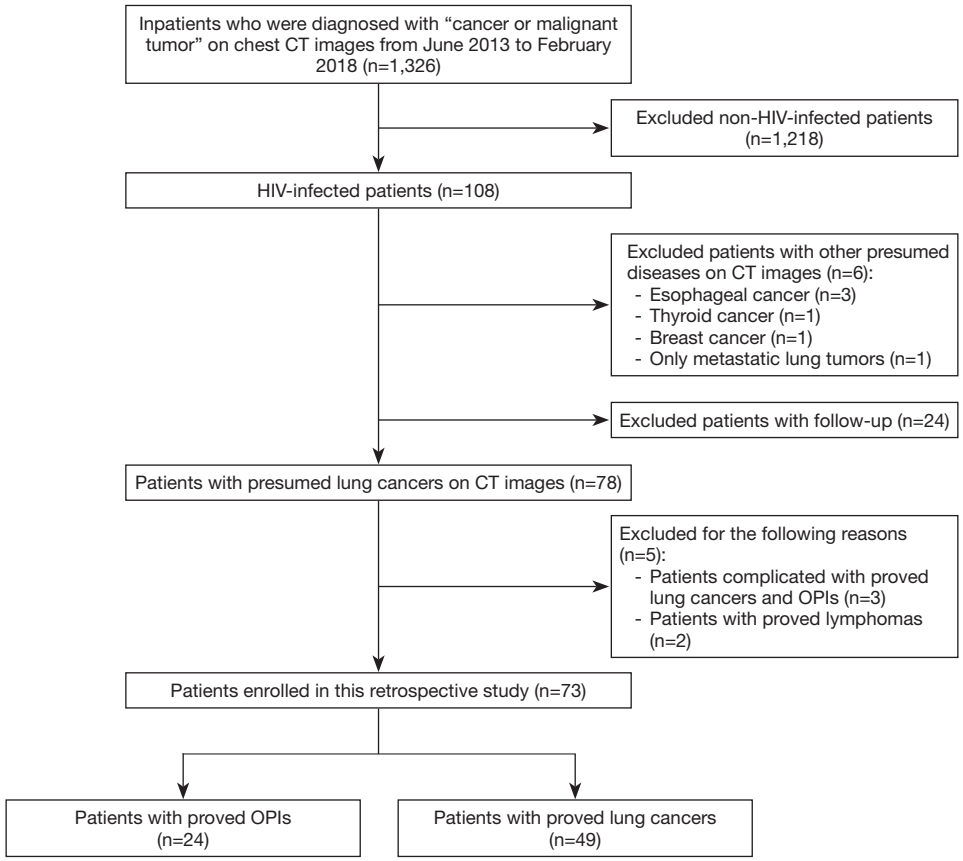

Figure 1 Patient selection flow chart. OPIs, opportunistic pulmonary infections.

radiologists.

OPIs mimicking malignancy and lung cancers were categorized as either peripheral- or central-type according to lesion locations on CT images. Peripheral-type lesions were distinctly separate from the mediastinum and hila, whereas central-type lesions were located in the mediastinum and/or hila and were directly associated with a segmental or larger airway (18).

All CT images were evaluated for lesion location and size (the maximal diameter on the transverse section), shape [regular (round or oval) or irregular], presence of internal calcification, cavitation or vacuole sign, pleural nodules or masses, pleural effusion, hydropericardium, and mediastinal and hilar adenopathy (nodes with short axes of at least 1 cm). In addition to the above, peripheral-type lesions were evaluated for border (lobulation, spiculation), presence of vascular convergence sign, CT bronchial sign, pleural indentation, and satellite lesions around the main lesion. In addition, central-type lesions were evaluated for adjacent obstructive pneumonia/atelectasis (19).

Radiomic features extraction

To minimize the variability of the CT attenuation value, enhanced CT images, which contributed a minor proportion of the total images, were not reviewed in this part. After cases with only enhanced-CT images were excluded, 22 patients with OPIs and 39 patients with lung cancers (40 main lesions) were included for radiomic analysis. Semiautomated segmentation of the lesion was implemented with our in-house software, which delineated the ROI on nonenhanced-CT images by points positioning and region growing methods. The lesion boundary was then adjusted manually by one radiologist (W Shi) and confirmed by another radiologist (F Shan). The ROI was delineated around the main lesion boundary on each transverse section. The bronchi and vessels were excluded. After segmentation, a total of 99 radiomic features were extracted with PyRadiomics, which is an open-source Python package (20). These CT-based radiomic features can be divided into six groups:

first order features, shape features, gray level cooccurrence matrix (GLCM) features, gray level size zone matrix (GLSZM) features, gray level run length matrix (GLRLM) features, and gray level dependence matrix (GLDM) features (20).

Statistical analysis

Statistical analysis was performed by R version 3.5.0 (R Project for Statistical Computing, Vienna, Austria). For quantitative variables, Wilcoxon rank-sum test was used because a majority of the data did not follow a normal distribution, and all of the variables were expressed as the median and interquartile range (IQR, 25th and 75th percentiles). The clinical characteristics (i.e., age at diagnosis, smoking index, HAART duration, $CD4^+$ counts, $CD4^+/CD8^+$ ratio), radiological features (i.e., lesion size) and all of the radiomic features of HIV-infected patients with OPIs were compared to those with lung cancers by Wilcoxon rank-sum test. Receiver operating characteristic (ROC) curves and area under the curves (AUC), including their 95% confidence intervals (95% CI), were used to evaluate the classification effects. The categorical variables including clinical characteristics (i.e., gender, proportion of smokers) and radiological features (all except lesion size) were expressed as number (percentage) of patients and analyzed by Fisher's exact test. Odds ratios (OR) and their 95% CI were also calculated. $P<0.05$ was considered to indicate a statistically significant difference.

Results

Diagnostic modalities

In the OPI group, 19 patients (79.2%) had tuberculosis (TB) infections, 2 (8.3%) had nontuberculosis mycobacterium (NTM) infections, 2 (8.3%) had cryptococcus infections and 1 (4.2%) had a mixed infection of TB and NTM. Among this group, nine patients with TB underwent an invasive diagnostic procedure [percutaneous CT-guided lung biopsy (4 patients); bronchoscopic biopsy (2 patients); resected specimen (3 patients)] for histological examination. Other patients with TB or NTM were diagnosed based on clinical and laboratory findings (i.e., mycobacterial smear and culture) and follow-up or treatment outcomes. Two patients (8.3%) with cryptococcus infections were diagnosed by percutaneous CT-guided lung biopsy.

In the 49 patients with lung cancers (50 main lesions), histological type was based on either tissues or cells from resected specimens (20 patients with 21 main lesions), percutaneous CT-guided lung biopsy (9 patients), bronchoscopic biopsy (7 patients), mediastinoscopic biopsy (2 patients), percutaneous biopsy of a metastatic lesion [7 patients (cervical lymph node biopsy in 6 patients, pleural nodule biopsy in 1 patient)], or pleural effusion cytology (4 patients). Tumor cell types included adenocarcinoma (24 patients), squamous cell carcinoma (15 patients with 16 main lesions), SCLC (5 patients), large cell carcinoma (3 patients), atypical carcinoid (1 patient), and poorly differentiated NSCLC (1 patient).

Eighteen patients (19 main lesions) with NSCLC (40.9%, 18/44 patients) were in advanced stages (15 at stage IV, 3 at stage IIIb), while the remaining 26 patients were in stages I–IIIa (9 at stage Ia, 3 at stage Ib, 1 at stage IIa, 7 at stage IIb, and 6 at stage IIIa). Five patients with SCLC had extensive disease.

Clinical features

The clinical characteristics of 24 HIV-infected patients with OPIs were compared to those of 49 HIV-infected patients with lung cancers (*Figure 2*). Patients with OPIs [41 (IQR, 36.8–52) years] were younger than those with cancers [58 (IQR, 51–63) years, P=0.000]. The proportion of smokers in patients with OPIs (8.3%, 2/24 patients) was lower than that in patients with cancers (36.7%, 18/49 patients, P=0.012), and smoking index in the former [0 (IQR, 0–0) pack-years] was lower than that in the latter [0 (IQR, 0–36) pack-years, P=0.007]. The HAART duration of patients with OPIs [0 (IQR, 0–0.2) months] was shorter than that of patients with cancers [8 (IQR, 0–32) months, P=0.002]. $CD4^+$ counts and $CD4^+/CD8^+$ ratio were profoundly diminished for the OPI group compared with the cancer group: 49.5 (IQR, 15.3–159.5) *vs.* 253 (IQR, 169–379) cells/μL, P=0.000 for $CD4^+$ counts; and 0.09 (IQR, 0.05–0.19) *vs.* 0.42 (IQR, 0.27–0.68), P=0.000 for the $CD4^+/CD8^+$ ratio. Gender make-up was not significantly different between the two groups.

CT morphological features

In the OPI group, all of the central-type lesions were caused by TB. When we compared CT features of the central-type lesions between the OPI and cancer groups, no significant differences were observed in their CT signs, which were listed in *Table 1* (*Figures 3*,*4*).

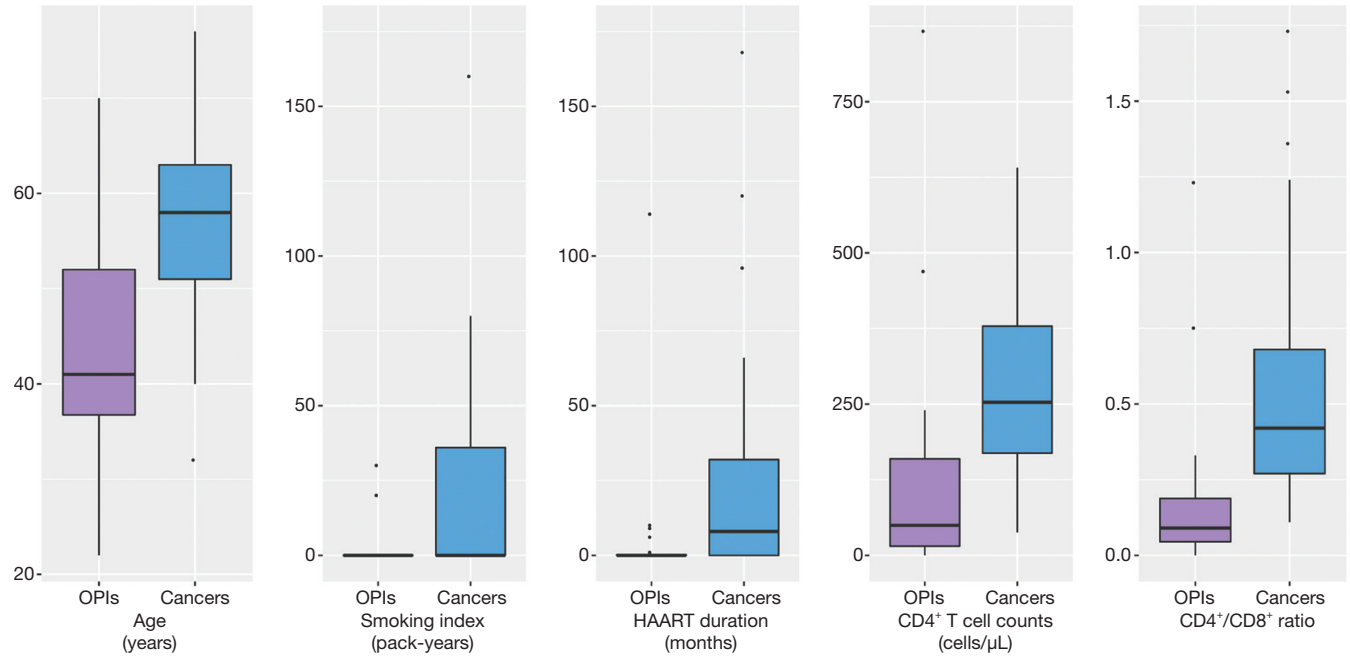

Figure 2 The box-and-whisker plot for clinical characteristics compared between the OPI and cancer groups. Using Wilcoxon rank-sum test, there were significant differences in age, smoking index, HAART duration, $CD4^+$ counts and $CD4^+/CD8^+$ ratio between the two groups ($P<0.05$ for all of the above). HAART, highly active antiretroviral therapy; OPIs, opportunistic pulmonary infections.

Table 1 CT morphological features of central-type lesions in HIV-infected patients with OPIs misdiagnosed as malignancy *vs.* those with lung cancers (n=29)

CT signs	OPIs (n=10), N (%)	Cancers (n=19), N (%)	P values	AUC (95% CI)	OR (95% CI)
Location					
Right lung	5 (50.0)	12 (63.2)	0.694	NA	0.59 (0.10–3.62)
Size (cm)	6.3 (4.4–6.9)	7.6 (6.2–8.6)	0.060	0.72 (0.52–0.92)	NA
Shape (irregular)	9 (90.0)	17 (89.5)	1.000	NA	1.06 (0.05–69.29)
Internal signs					
Calcification	3 (30.0)	2 (10.5)	0.306	NA	3.47 (0.32–50.17)
Vacuole sign	3 (30.0)	2 (10.5)	0.306	NA	3.47 (0.32–50.17)
Cavitation	0 (0.0)	2 (10.5)	0.532	NA	0.00 (0.00–10.24)
Adjacent structural changes					
Obstructive pneumonia	8 (80.0)	12 (63.2)	0.431	NA	2.27 (0.31–27.92)
Obstructive atelectasis	4 (40.0)	13 (68.4)	0.236	NA	0.32 (0.05–1.95)
Pleural nodules or masses	0 (0.0)	3 (15.8)	0.532	NA	0.00 (0.00–4.61)
Pleural effusion	3 (30.0)	10 (52.6)	0.433	NA	0.40 (0.05–2.45)
Hydropericardium	1 (10.0)	6 (31.6)	0.367	NA	0.25 (0.00–2.67)
Lymphadenopathy	10 (100.0)	19 (100.0)	1.000	NA	0.00 (0.00–Inf)

Data were presented as a median (interquartile range) or number (percentage); 95% CI, 95% confidence intervals; AUC, area under the (receiver operating characteristic) curve; Inf, infinite; NA, not available; OPIs, opportunistic pulmonary infections; OR, odds ratios.

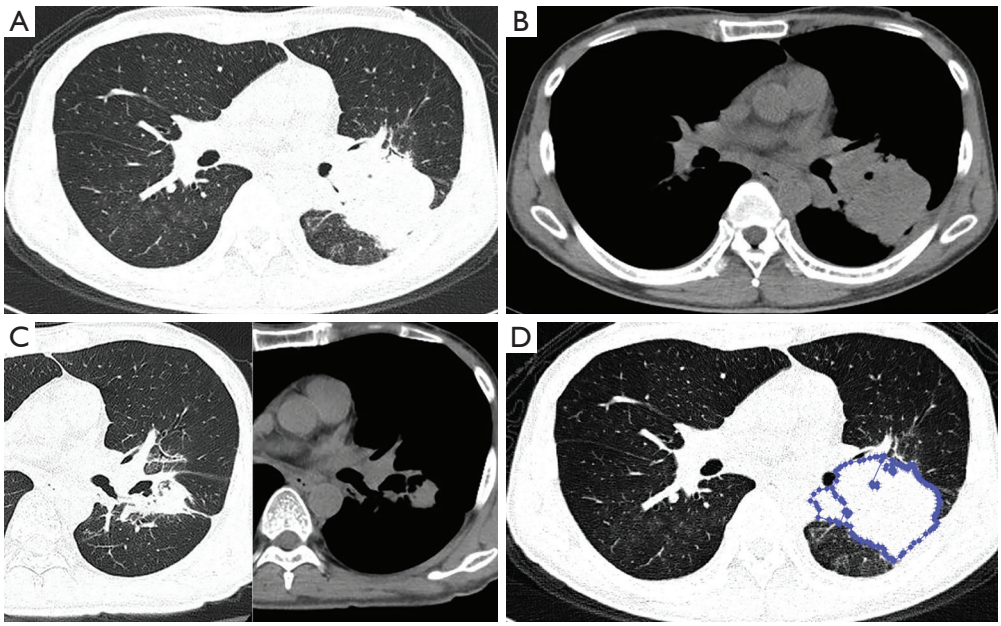

Figure 3 A 42-year-old male complained of cough and sputum with fever for more than 2 months. He had a CD4$^+$ count of 8 cells/μL and was presently diagnosed with HIV infection. Nonenhanced CT with lung window (A) and mediastinal window (B) settings showed mass-like consolidation located in the left hila, with a presumptive diagnosis of neoplasm and had lung TB confirmed by bronchoscopic biopsy with no evidence of malignancy. (C) After antiretroviral therapy and anti-tuberculous therapy for more than 1 month, CT showed that the pulmonary lesions were obviously absorbed. (D) One image from this case, segmented with semiautomated software and manually adjusted by radiologists. TB, tuberculosis.

Figure 4 A 53-year-old male complained of chest tightness and dyspnea for 2 weeks. He had been receiving highly active antiretroviral therapy for more than 24 months and had a CD4$^+$ count of 281 cells/μL. Nonenhanced CT with lung window (A) and mediastinal window (B) settings showed consolidation with adjacent obstructive pneumonia/atelectasis located in the left upper lobe, multiple lung metastases, pleural effusion, and adenopathy. Adenocarcinoma was then histologically confirmed by pleural effusion cytology. (C) One image from this case, segmented with semiautomated software and manually adjusted by radiologists.

With regard to CT features of the peripheral-type lesions, the presence of pleural indentation was less common in the OPI group (7.1%, 1/14 cases) than in the cancer group (45.2%, 14/31 cases, P=0.016), and the presence of satellite lesions was more common in the OPI group (50.0%, 7/14 cases) than in the cancer group (12.9%, 4/31 cases, P=0.020). No significant differences between the two groups were observed in other CT features of peripheral-type lesions, which were listed in *Table 2* (*Figures 5*,*6*).

Table 2 CT morphological features of peripheral-type lesions in HIV-infected patients with OPIs misdiagnosed as malignancy *vs.* those with lung cancers (n=45)

CT signs	OPIs (n=14), N (%)	Cancers (n=31), N (%)	P values	AUC (95% CI)	OR (95% CI)
Location					
Right lung	9 (64.3)	20 (64.5)	1.000	NA	0.99 (0.22–4.75)
Superior lobe	9 (64.3)	16 (51.6)	0.525	NA	1.67 (0.39–7.89)
Size (cm)	2.4 (1.4–4.8)	3.2 (2.5–4.6)	0.339	0.59 (0.37–0.81)	NA
Shape (irregular)	5 (35.7)	6 (19.4)	0.277	NA	2.27 (0.43–11.68)
Border					
Lobulation	9 (64.3)	27 (87.1)	0.111	NA	0.28 (0.04–1.59)
Spiculation	7 (50.0)	23 (74.2)	0.172	NA	0.36 (0.08–1.60)
Internal signs					
Calcification	1 (7.1)	2 (6.5)	1.000	NA	1.11 (0.02–23.21)
Vacuole sign	2 (14.3)	3 (9.7)	0.639	NA	1.54 (0.11–15.33)
Cavitation	0 (0.0)	1 (3.2)	1.000	NA	0.00 (0.00–86.24)
Adjacent structural changes					
Vascular convergence sign	6 (42.9)	16 (51.6)	0.749	NA	0.71 (0.16–2.98)
CT bronchial sign	7 (50.0)	18 (58.1)	0.749	NA	0.73 (0.17–3.10)
Pleural indentation	1 (7.1)	14 (45.2)	0.016*	NA	0.10 (0.00–0.80)
Satellite lesions	7 (50.0)	4 (12.9)	0.020*	NA	6.40 (1.23–39.42)
Pleural nodules or masses	1 (7.1)	3 (9.7)	1.000	NA	0.72 (0.01–10.04)
Pleural effusion	5 (35.7)	5 (16.1)	0.244	NA	2.81 (0.52–15.64)
Hydropericardium	3 (21.4)	1 (3.2)	0.082	NA	7.75 (0.56–442.07)
Lymphadenopathy	7 (50.0)	15 (48.4)	1.000	NA	1.07 (0.25–4.54)

Data were presented as a median (interquartile range) or number (percentage). *, P<0.05 patients with OPIs *vs.* patients with lung cancers; 95% CI, 95% confidence intervals; AUC, area under the (receiver operating characteristic) curve; Inf, infinite; NA, not available; OPIs, opportunistic pulmonary infections; OR, odds ratios.

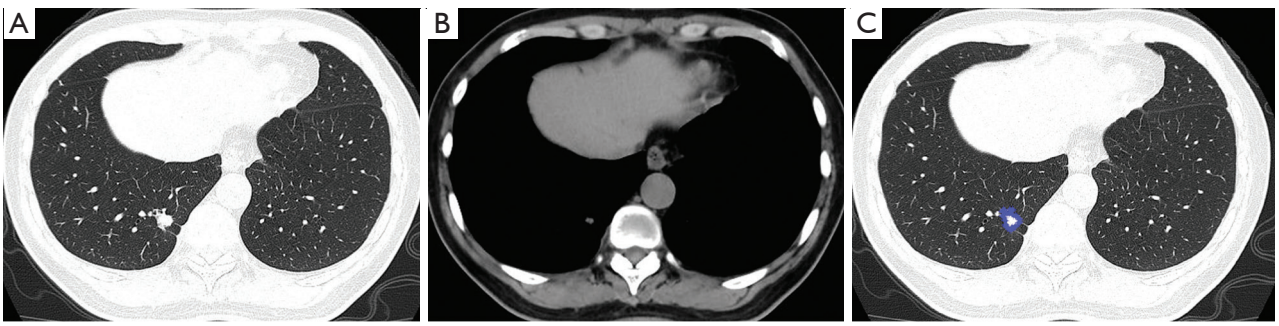

Figure 5 A 52-year-old male complained of a pulmonary nodule found by physical examination for 2 months. He had been receiving highly active antiretroviral therapy for more than 9 years and had a $CD4^+$ count of 866 cells/μL. Nonenhanced CT with lung window (A) and mediastinal window (B) settings showed a solid nodule with lobulation, spiculation and pleural indentation located in the right lower lobe, which was initially misdiagnosed as lung cancer and then histologically confirmed to be tuberculoma by wedge resection. (C) One image from this case, segmented with semiautomated software and manually adjusted by radiologists.

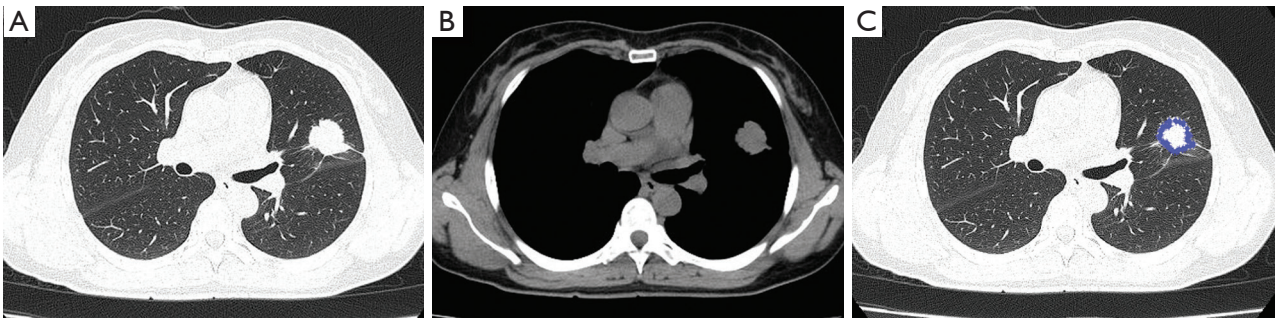

Figure 6 A 51-year-old female complained of a pulmonary nodule found by physical examination for 3 weeks. She had been receiving highly active antiretroviral therapy for more than 8 years and had a $CD4^+$ count of 319 cells/μL. Nonenhanced CT with lung window (A) and mediastinal window (B) settings showed a solid nodule with lobulation, spiculation and pleural indentation located in the left upper lobe. Mucinous adenocarcinoma was confirmed by lobectomy. (C) One image from this case, segmented with semiautomated software and manually adjusted by radiologists.

Table 3 CT-based radiomic features of central-type lesions in HIV-infected patients with OPIs misdiagnosed as malignancy *vs.* those with lung cancers (n=25)

Radiomic parameters	OPIs (n=10)	Cancers (n=15)	P values	AUC (95% CI)
Large dependence high gray level emphasis (LDHGLE)	22,007.46 (18,006.74–23,778.02)	9,986.32 (7,726.40–12,744.84)	0.008*	0.93 (0.84–1.00)
Skewness	−0.95 (−1.15 to −0.59)	−0.05 (−0.29 to −0.02)	0.017*	0.89 (0.77–1.00)
Inverse difference normalized (IDN)	0.95 (0.94–0.95)	0.93 (0.92–0.93)	0.017*	0.89 (0.76–1.00)
Kurtosis	8.12 (7.46–9.97)	3.55 (3.27–5.39)	0.017*	0.89 (0.75–1.00)
90 percentiles	132.00 (121.00–140.50)	183.00 (149.50–205.50)	0.059	0.86 (0.69–1.00)

Data were presented as a median (interquartile range); P values above were adjusted using false discovery rate (FDR) method to correct for multiple testing; *, P<0.05 patients with OPIs *vs.* patients with lung cancers; 95% CI, 95% confidence intervals; AUC, area under the (receiver operating characteristic) curve; OPIs, opportunistic pulmonary infections.

CT-based radiomic features

All of the central-type lesions analyzed by radiomics were solid lesions. According to P values and AUC values, the first five radiomic parameters of central-type lesions compared between the OPI and cancer groups were listed in *Table 3*. Four radiomic parameters of central-type lesions were significantly different, including large dependence high gray level emphasis (LDHGLE), skewness, inverse difference normalized (IDN) and kurtosis. These four radiomic parameters had AUCs of 0.93, 0.89, 0.89, and 0.89 (P=0.008, 0.017, 0.017, and 0.017, respectively) (*Figure 7*). Except for the solid lesions, the peripheral-type lesions analyzed by radiomics also contained one case of pure ground glass nodules (pGGN) due to OPI and four cases of mixed ground glass nodules (mGGN) due to cancers. No significant differences were found in radiomic parameters of peripheral-type lesions between the OPI and cancer groups (*Table 4*).

Discussion

Our hospital is the only tertiary referral hospital for HIV-infected populations in Shanghai, China. Each year, approximately more than 600 patients with HIV are referred to our hospital. We conducted a retrospective study, covering a 5-year period, of HIV-infected patients who had presumed lung cancer but turned out to have pulmonary infection instead. Although we tried to include as many subjects as possible, the number of HIV-infected patients with OPIs mimicking lung cancers was small. TB infections accounted for 79.2% of those patients, NTM infections for 8.3%, cryptococcus infections for 8.3%, and a mixed infection of TB and NTM for 4.2%.

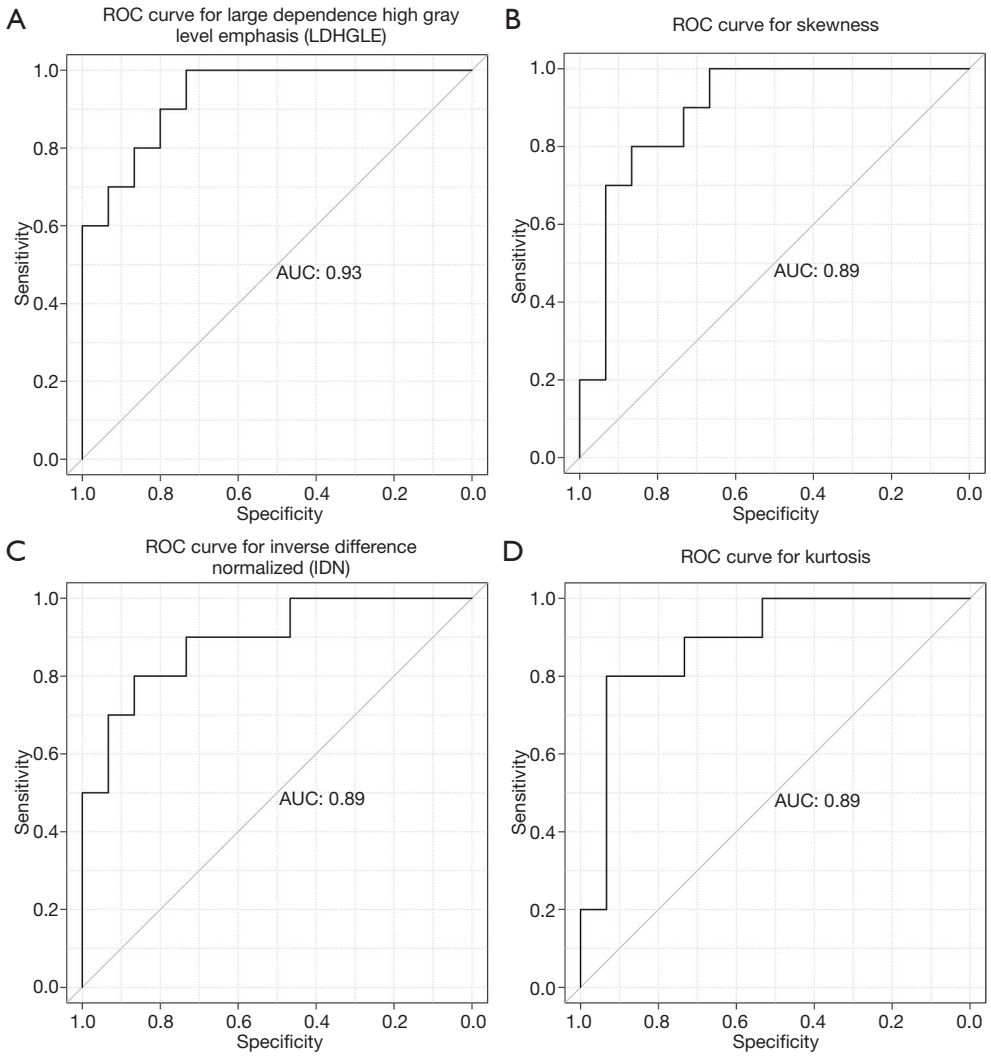

Figure 7 Receiver operating characteristic (ROC) curves of the four significant radiomic parameters of central-type lesions used to distinguish between opportunistic pulmonary infections and lung cancers, including large dependence high gray level emphasis (LDHGLE) (A), skewness (B), inverse difference normalized (IDN) (C) and kurtosis (D) (P<0.05 for all of the above).

Table 4 CT-based radiomic features of peripheral-type lesions in HIV-infected patients with OPIs misdiagnosed as malignancy *vs.* those with lung cancers (n=37)

Radiomic parameters	OPIs (n=12)	Cancers (n=25)	P values	AUC (95% CI)
Joint entropy	7.51 (6.51–8.26)	8.48 (7.74–8.92)	0.931	0.71 (0.54–0.88)
Dependence entropy	6.14 (5.81–6.42)	6.42 (6.21–6.56)	0.931	0.71 (0.52–0.90)
Joint energy	7.36E−03 (4.68E−03 to 1.79E−02)	4.40E−03 (3.30E−03 to 7.09E−03)	0.931	0.71 (0.54–0.88)
Total energy	1.47E+08 (5.58E+07 to 6.45E+08)	2.92E+08 (1.91E+08 to 6.32E+08)	0.931	0.67 (0.45–0.88)
Zone entropy	5.99 (5.6–6.35)	6.30 (6.14–6.39)	0.931	0.67 (0.46–0.87)

Data were presented as a median (interquartile range); P values above were adjusted using false discovery rate (FDR) method to correct for multiple testing; 95% CI, 95% confidence intervals; AUC, area under the (receiver operating characteristic) curve; OPIs, opportunistic pulmonary infections.

Rolston *et al.* conducted a large study of general population in 2,908 patients who underwent biopsy with a presumed diagnosis of lung cancer, 37 of whom were found to have infections (3). Fungal infection was the most common, accounting for 46% of the infections diagnosed, followed by mycobacteria accounting for 27%. Pitlik *et al.* reported on 26 cases out of more than 70,000 patients who were referred to the Texas Cancer Center, USA during a 10-year period with presumptive diagnosis of neoplasm that was proved bacteriologically to be TB with no evidence of malignancy (21). A limited number of other studies have reported pulmonary infections, primarily including TB (4,5,22), fungus (6) and NTM (5,7) infections, that mimicked lung cancers. These studies indicate that the incidence of pulmonary infections masquerading as cancers is infrequent and that the specific disease spectrum of infections may be related to the immune status of the study populations or regional incidence.

In our study, most patients with OPIs were younger men, who had lower $CD4^+$ counts and were diagnosed with HIV coinfection without initiating HAART. These conditions may be related to HIV epidemiology in China. Migrant populations are recognized as one of the groups most affected by HIV, of whom approximately half are registered, nonpermanent residents working in the most quickly developing regions. Most of these individuals are young men, and the overall prevalence of HIV among men who have sex with men (MSM) is on the rise in recent years (23). The open nature of Chinese economy has made it difficult to monitor and control internal migration. Floating populations are the most difficult to reach with preventive health education, and they tend to be deprived of access to health care (24). This means that such individuals with HIV may be in severe immunosuppression once they are identified.

In addition, HAART has elongated the life spans of people living with HIV/AIDS, and the HIV-infected population is aging. Lung cancer is one of the most common non-AIDS-defining malignancies among HIV-infected patients. The incidence of lung cancer has significantly increased in the HAART era (25,26). Similar to a previous report (27), our study found that HIV-infected patients with lung cancer were relatively elderly. They reported more tobacco consumption in the current study. Research has reported that the risk of smoking-related cancers is much higher in HIV-infected smokers compared with both the general population and HIV-infected nonsmokers, and lung cancer is one of the major types of cancer observed in HIV-infected smokers (28).

In our study, all central-type OPIs caused by TB, which were primary TB radiologically mimicking central-type lung cancer, presented with lymphadenopathy, consolidation, pleural effusion, consistent with the results reported in previous studies (29,30). The CT features of central-type lesions due to OPIs in our study overlapped with those of primary lung cancer, and the differences between the two groups fell short of statistical significance. This result might be explained because the sample size of patients with central-type lesions was limited. Radiologists often make judgments based on conventional diagnostic ideas leading to misdiagnosis of these types of OPIs; that is, large hilar masses suggest a greater chance of malignancy.

The majority of peripheral-type OPIs were caused by TB, followed by NTM and cryptococcus infections in the present study. Post-primary TB has varied presentations, which include nodules, tuberculoma, cavity, cicatrization, aspergilloma, bronchiectasis, pleural effusion, mediastinal adenopathy and end-stage lung destruction (29,31). NTM pulmonary diseases are classified into upper-lobe fibrocavitary disease and nodular bronchiectatic disease according to radiologic patterns. Characteristic radiologic features of fibrocavitary disease include heterogeneous nodular and cavitary opacities in the upper lobes, whereas those of nodular bronchiectatic disease are bronchiectasis and branching centrilobular nodules in the middle lobe and lingual (32). Cryptococcus infections may radiographically manifest as a solitary lung nodule or mass, multiple nodules, segmental or lobar consolidation, or, rarely, interstitial pneumonia. Associated features include cavitation, lymphadenopathy and pleural effusion (33). Our study showed that peripheral-type OPIs manifested as solitary pulmonary nodules (SPNs) or masses with few alleged typical imaging features of infections listed above, which might be a potential cause of misdiagnosis of OPIs as malignancy on CT images.

Pleural indentation is a well-known radiological sign on chest CT that suggests a possible pleural invasion by peripheral NSCLC (34). It is associated with internal tissue fibrosis traction on the neighboring tissue structure, which is more common in adenocarcinoma (34). Pleural indentation is also observed in inflammatory granulomas, especially tuberculomas. In our study, the frequency of pleural indentation was significantly higher in patients with cancers than in patients with OPIs (P=0.016). However, using pleural indentation to identify benign and malignant cases is controversial (35). We believe that differences in the baseline characteristics, i.e., SPNs size and pathological

type may have resulted in the different outcomes observed in various studies. While it is not specific to diagnose lung cancer relying only on pleural indentation (35), pleural indentation in combination with various signs will elevate the specificity and positive prediction rate for better differentiation.

Satellite lesions are usually described as small discrete shadows in the immediate vicinity of the main lesion. The presence of satellite nodules is characteristic of granulomatous disease and is estimated to have a positive predictive value (PPV) of 90% for a benign etiology (36). In our study, OPIs frequently showed satellite lesions (P=0.020), which could be helpful for differentiation from lung cancer, consistent with previous studies (37,38). Even so, the presence of satellite nodules does not allow confident diagnosis of benignity, as 10% of dominant nodules with satellite nodules will be malignant. When cancerous, satellite nodules are usually the result of peripheral foci of tumor or skip metastatic lesions (39).

Skewness measures the asymmetry of the distribution of values about the mean value (20). In our study, the distribution of central-type lesions in the OPI and cancer groups was negatively skewed, and the absolute value of such lesions in the OPI group was significantly greater than that in the cancer group (P=0.017). This implied that the OPI group had a distribution of more voxels of low gray-level values relative to the group's mean value. Just as for skewness, kurtosis is a descriptor of the shape of a probability distribution, which is another way of quantifying it for a theoretical distribution (20). In our study, the kurtosis of central-type lesions in the OPI group was significantly greater than that in the cancer group (P=0.017). This implied that the OPI group had a more skewed distribution, which was consistent with the measures of skewness obtained. This is because the pathologic basis of central-type lesions due to OPIs (i.e., TB) is necrotic mass-like granuloma with infiltration of inflammatory cells or caseating pneumonia with granuloma (40). The patients with OPIs had low $CD4^+$ counts leading to impairment of granuloma formation (41). Therefore, there might have been fewer areas of granuloma representing high gray-level values and relatively more areas of caseating pneumonia or necrosis representing low gray-level values in the lesions. LDHGLE and IDN are higher-order statistical features that describe gray-value spatial interrelationships and thus reflect the texture characteristics of lung nodules or masses (42). A higher LDHGLE implies that more voxels of high gray-level values are adjacent to each other (20). In our study, the LDHGLE of central-type lesions in the OPI group was significantly greater than that in the cancer group (P=0.008). This can be explained by the fact that several tissue components, such as coagulation and liquefactive necrosis, are dispersed within the parenchyma component of lung cancers in various combinations (43), so that the density of the solid component of tumor is more inhomogeneous than that of OPIs; in other words, high gray-level values in OPIs are concentrated together more than those in lung cancers. Similarly, the higher IDN is, the more homogeneous the local image (20). In our study, IDN of central-type lesions in the OPI group was significantly higher than that in the cancer group (P=0.017), representing homogeneity of the OPIs.

There were no significant differences in the radiomic parameters of peripheral-type lesions between the two groups. This might be because both solid and subsolid [pGGN due to OPI (8.3%, 1/12 cases) and mGGN due to cancer (16.0%, 4/25 cases)] nodules or masses were included in the radiomic analysis, because peripheral-type OPIs caused by several pathogens (TB, NTM or cryptococcus) had more variability, or because differences between the two groups were not revealed by nonenhanced-CT-based radiomic analysis.

Our study has several limitations. First, because the incidence of pulmonary infections masquerading as cancers is infrequent, the sample size of this study was relatively small. In the future, larger sample sizes can be achieved through prospective multicenter research. Second, the CT acquisition protocol was not completely standardized across the patients. This might result in variability in CT attenuation values with resultant biases in the radiomic analysis. Third, lesion segmentation was implemented with semiautomated software and manual adjustment by radiologists with certain biases. However, this should be an acceptable way to approach segmentation, as fully automatic segmentation is difficult to implement at present.

In conclusion, HIV-infected patients with OPIs can present with radiological findings similar to lung cancers. Clinicoradiologic characteristics together with radiomic features may help identify OPIs mimicking lung cancers in HIV-infected patients. The initial application of CT radiomics in OPIs and cancers may provide added diagnostic value for differentiation, especially in central-type lesions. In the future, we should increase the sample size, standardize the CT acquisition protocol and improve the automatic segmentation method to further improve the accuracy of diagnosis through prospective multicenter research.

Acknowledgments

Funding: This work was supported by the Intelligent Medical Special Research Foundation of the Shanghai Health and Family Planning Commission (No. 2018ZHYL0104) and the National Natural Science Foundation of China (No. 81601634).

Footnote

Conflicts of Interest: The authors have no conflicts of interest to declare.

Ethical Statement: The Institutional Review Board of Shanghai Public Health Clinical Center, Fudan University approved this retrospective study (No. 2019-S018-01), with a waiver of informed consent.

References

1. Chou SH, Prabhu SJ, Crothers K, et al. Thoracic diseases associated with HIV infection in the era of antiretroviral therapy: clinical and imaging findings. Radiographics 2014;34:895-911.
2. Benito N, Moreno A, Miro JM, et al. Pulmonary infections in HIV-infected patients: an update in the 21st century. Eur Respir J 2012;39:730-45.
3. Rolston KV, Rodriguez S, Dholakia N, et al. Pulmonary infections mimicking cancer: a retrospective, three-year review. Support Care Cancer 1997;5:90-3.
4. Hammen I. Tuberculosis mimicking lung cancer. Respir Med Case Rep 2015;16:45-7.
5. Hahm CR, Park HY, Jeon K, et al. Solitary pulmonary nodules caused by Mycobacterium tuberculosis and Mycobacterium avium complex. Lung 2010;188:25-31.
6. Gazzoni FF, Severo LC, Marchiori E, et al. Fungal diseases mimicking primary lung cancer: radiologic-pathologic correlation. Mycoses 2014;57:197-208.
7. Hong SJ, Kim TJ, Lee JH, et al. Nontuberculous mycobacterial pulmonary disease mimicking lung cancer: Clinicoradiologic features and diagnostic implications. Medicine (Baltimore) 2016;95:e3978.
8. Lambin P, Rios-Velazquez E, Leijenaar R, et al. Radiomics: extracting more information from medical images using advanced feature analysis. Eur J Cancer 2012;48:441-6.
9. Gillies RJ, Kinahan PE, Hricak H. Radiomics: Images Are More than Pictures, They Are Data. Radiology 2016;278:563-77.
10. Limkin EJ, Sun R, Dercle L, et al. Promises and challenges for the implementation of computational medical imaging (radiomics) in oncology. Ann Oncol 2017;28:1191-206.
11. Lee G, Lee HY, Park H, et al. Radiomics and its emerging role in lung cancer research, imaging biomarkers and clinical management: State of the art. Eur J Radiol 2017;86:297-307.
12. Chen CH, Chang CK, Tu CY, et al. Radiomic features analysis in computed tomography images of lung nodule classification. PLoS One 2018;13:e0192002.
13. Hawkins S, Wang H, Liu Y, et al. Predicting Malignant Nodules from Screening CT Scans. J Thorac Oncol 2016;11:2120-8.
14. Lee SH, Lee SM, Goo JM, et al. Usefulness of texture analysis in differentiating transient from persistent part-solid nodules(PSNs): a retrospective study. PLoS One 2014;9:e85167.
15. Chae HD, Park CM, Park SJ, et al. Computerized texture analysis of persistent part-solid ground-glass nodules: differentiation of preinvasive lesions from invasive pulmonary adenocarcinomas. Radiology 2014;273:285-93.
16. Detterbeck FC, Boffa DJ, Kim AW, et al. The Eighth Edition Lung Cancer Stage Classification. Chest 2017;151:193-203.
17. Carter BW, Glisson BS, Truong MT, et al. Small cell lung carcinoma: staging, imaging, and treatment considerations. Radiographics 2014;34:1707-21.
18. Fishman JE, Schwartz DS, Sais GJ, et al. Bronchogenic carcinoma in HIV-positive patients: findings on chest radiographs and CT scans. AJR Am J Roentgenol 1995;164:57-61.
19. Hansell DM, Bankier AA, MacMahon H, et al. Fleischner Society: glossary of terms for thoracic imaging. Radiology 2008;246:697-722.
20. van Griethuysen JJM, Fedorov A, Parmar C, et al. Computational Radiomics System to Decode the Radiographic Phenotype. Cancer Res 2017;77:e104-7.
21. Pitlik SD, Fainstein V, Bodey GP. Tuberculosis mimicking cancer--a reminder. Am J Med 1984;76:822-5.
22. Prytz S, Hansen JL. A follow-up examination of patients with pulmonary tuberculosis resected on suspicion of tumour. Scand J Respir Dis 1976;57:239-46.
23. Han J, Tian X, Yu G, et al. Disclosure Pattern of Self-Labeled People Living with HIV/AIDS on Chinese Social Networking Site: An Exploratory Study. Cyberpsychol Behav Soc Netw 2016;19:516-23.
24. Mi G, Ma B, Kleinman N, et al. Hidden and Mobile: A Web-based Study of Migration Patterns of Men

Who Have Sex with Men in China. Clin Infect Dis 2016;62:1443-7.
25. Engels EA, Biggar RJ, Hall HI, et al. Cancer risk in people infected with human immunodeficiency virus in the United States. Int J Cancer 2008;123:187-94.
26. Helleberg M, Gerstoft J, Afzal S, et al. Risk of cancer among HIV-infected individuals compared to the background population: impact of smoking and HIV. AIDS 2014;28:1499-508.
27. Hou W, Fu J, Ge Y, et al. Incidence and risk of lung cancer in HIV-infected patients. J Cancer Res Clin Oncol 2013;139:1781-94.
28. Jin ZY, Liu X, Ding YY, et al. Cancer risk factors among people living with HIV/AIDS in China: a systematic review and meta-analysis. Sci Rep 2017;7:4890.
29. Nachiappan AC, Rahbar K, Shi X, et al. Pulmonary Tuberculosis: Role of Radiology in Diagnosis and Management. Radiographics 2017;37:52-72.
30. Burrill J, Williams CJ, Bain G, et al. Tuberculosis: a radiologic review. Radiographics 2007;27:1255-73.
31. Kim HY, Song KS, Goo JM, et al. Thoracic sequelae and complications of tuberculosis. Radiographics 2001;21:839-58; discussion 859-60.
32. Kim TS, Koh WJ, Han J, et al. Hypothesis on the evolution of cavitary lesions in nontuberculous mycobacterial pulmonary infection: thin-section CT and histopathologic correlation. AJR Am J Roentgenol 2005;184:1247-52.
33. Fox DL, Muller NL. Pulmonary cryptococcosis in immunocompetent patients: CT findings in 12 patients. AJR Am J Roentgenol 2005;185:622-6.
34. Ji M, Zhang Y, Shi B, et al. Association of promoter methylation with histologic type and pleural indentation in non-small cell lung cancer (NSCLC). Diagn Pathol 2011;6:48.
35. Kuhlman JE, Fishman EK, Kuhajda FP, et al. Solitary bronchioloalveolar carcinoma: CT criteria. Radiology 1988;167:379-82.
36. Soubani AO. The evaluation and management of the solitary pulmonary nodule. Postgrad Med J 2008;84:459-66.
37. Kim H, Kang SJ, Suh GY, et al. Predictors for benign solitary pulmonary nodule in tuberculosis-endemic area. Korean J Intern Med 2001;16:236-41.
38. Seemann MD, Staebler A, Beinert T, et al. Usefulness of morphological characteristics for the differentiation of benign from malignant solitary pulmonary lesions using HRCT. Eur Radiol 1999;9:409-17.
39. Winer-Muram HT. The solitary pulmonary nodule. Radiology 2006;239:34-49.
40. Lee JY, Lee KS, Jung KJ, et al. Pulmonary tuberculosis: CT and pathologic correlation. J Comput Assist Tomogr 2000;24:691-8.
41. Scott L, da Silva P, Boehme CC, et al. Diagnosis of opportunistic infections: HIV co-infections - tuberculosis. Curr Opin HIV AIDS 2017;12:129-38.
42. Bashir U, Siddique MM, McLean E, et al. Imaging Heterogeneity in Lung Cancer: Techniques, Applications, and Challenges. AJR Am J Roentgenol 2016;207:534-43.
43. Quaia E, Baratella E, Pizzolato R, et al. Radiological-pathological correlation in intratumoural tissue components of solid lung tumours. Radiol Med 2009;114:173-89.

Cite this article as: Shi W, Zhou L, Peng X, Ren H, Wang Q, Shan F, Zhang Z, Liu L, Shi Y. HIV-infected patients with opportunistic pulmonary infections misdiagnosed as lung cancers: the clinicoradiologic features and initial application of CT radiomics. J Thorac Dis 2019;11(6):2274-2286. doi: 10.21037/jtd.2019.06.22

